

A parameter-free statistical measurement of halos with power spectra

Ping He^{1,2}, Long-Long Feng^{1,3} and Li-Zhi Fang²

ABSTRACT

We show that in the halo model of large-scale structure formation, the difference between the Fourier and the discrete wavelet transform (DWT) power spectra provides a statistical measurement of the halos. This statistical quantity is free from parameters related to the shape of the mass profile and the identification scheme of the halos. That is, the statistical measurement is invariant in the sense that models with reasonably defined and selected parameters of the halo models should yield the same difference of the Fourier and DWT spectra. This feature is useful to extract ensemble-averaged properties of halos, which cannot be obtained with the identification of individual halos. To demonstrate this point, we show with WIGEON hydrodynamic simulation samples that the spectrum difference provides a quantitative measurement of the discrepancy of the distribution of baryonic gas from that of the underlying dark matter field within halos. We also show that the mass density profile of halos in physical space can be reconstructed with this statistical measurement. This profile essentially is the average over an ensemble of halos, including well-virialized halos, as well as halos with significant internal substructures. Moreover, this reconstruction is sensitive to the tail of the mass density profile. We showed that the profile with a $1/r^3$ tail gives very different result from that with $1/r^2$. Other possible applications of this method are discussed as well.

Subject headings: cosmology: theory - large-scale structure of the universe

¹National Astronomical Observatories, Chinese Academy of Science, Chao-Yang District, Beijing, 100012, P.R. China

²Department of Physics, University of Arizona, Tucson, AZ 85721

³Purple Mountain Observatory, Nanjing 210008, P.R. China

1. Introduction

The dynamical equations of cosmic collisionless particles (dark matter) do not have preferred scales. Therefore, if the initial density perturbations are Gaussian and scale-free, the equations admit a self-similar solution, and the cosmic clustering of dark matter has to be scale-invariant (Peebles 1980). To sketch this clustering, the halo model assumes that the cosmic mass field in the nonlinear regime is given by a superposition of the halos on various spatial scales. The halo-halo correlation function on scales larger than the halo size is given by the two-point correlation function of the initially linear Gaussian field. In the early version of the halo model, the mass density profile of the halos is supposed to be self-similar. For instance, in the model of Neyman & Scott (1952), the distribution of galaxies within various clusters is assumed to obey the same probability law, which is independent of the mass of clusters. Scherrer & Bertschinger (1991) used a scale-free function $g(x)$ to model the density profile $f(m, x) = mg(x)$ of a mass m halo. In the current halo model, the halos are generally described by the universal mass profiles. There are several different versions of the profiles (Hernquist 1990; Navarro et al. 1996; Moore et al. 1999). A common feature of these halo density profiles is that the parameters used in the density profiles are either mass-independent or dependent on mass approximately by a power law. Therefore these density profiles essentially scale with respect to halo mass.

The halo model has been extensively applied to modeling the hierarchical formation of galaxies and other objects (e.g., Wang et al. 2004 and references therein). It tries to explain the formation and evolution of galaxies with the mass function, the universal density profile, two-point correlations of host halos, and the bias model of the relevant objects (e.g., Cooray & Sheth 2002 and references therein).

The basic assumptions of the halo model are correct only statistically. Previous N -body simulations show that the shapes of halos are often nonspherical and that the parameters of mass profiles of halos are dependent on the halo mass. For instance, probably no more than 70% of halos can be fitted by the universal mass profile. There is a considerable amount of variation in the density profile even among the halos that can be fitted by the universal mass profile (Jing 2000; Bullock et al. 2001). The universality of spherically symmetric profiles is approximately valid for the average over ensembles of halos but not so for individual halos. Moreover, the mass function of halos also depends on halo finders (Jenkins et al. 2001). That is, the ensembles of halos with a given mass do not completely depend on mass but also depend on the parameters used in the halo identification. This may lead to assigning different properties to halos at a given mass because the masses are assigned using a different algorithm. Thus, it would not be trivial in comparing halo catalogs constructed using two different halo identification schemes.

Obviously, the parameters of the halo finder should be irrelevant to physical conclusions yielded from the halo model. Therefore, it would be significant to directly measure the ensemble-averaged properties of halos without invoking *a priori* parameters related to the details of mass profiles and the specific halo finders. In this paper, we propose a parameter-free statistical scheme to measure the halos. It relies only on the physical essence of the halo model and not on the assumptions of the shape of the halos. This measurement is based on a relation between the power spectra of Fourier and discrete wavelet transform (DWT) bases. For Gaussian fields with either colored or white spectra, the Fourier and the DWT power spectra are equivalent to each other; that is, the Fourier power spectrum $P(n)$ can be transferred to the DWT power spectrum P_j and vice versa. Yet, for non-Gaussian fields, the Fourier and the DWT power spectra are no longer equivalent. The difference between the Fourier and the DWT power spectra completely comes from the non-Gaussianity of the field. Thus, if the non-Gaussianity of a mass field is caused by halos, the difference between the Fourier and the DWT power spectra provides a direct statistical measurement of halos.

The paper is organized as follows. In §2, we derive the relation between the Fourier and the DWT power spectra and show that the difference between the Fourier and the DWT power spectra provides the ensemble-averaged measurement of halo profiles. §3 describes the samples used for demonstration. §4 demonstrates the possible applications of this measure, including (1) the distribution of baryonic gas in halos and (2) the reconstruction of the halo mass profile. The discussion and conclusion are given in §5.

2. Theory

2.1. The Fourier and DWT power spectra

To show the essence of the method, we consider a one-dimensional random density distribution $\rho(x)$ in the range $0 < x < L$. It is straightforward to generalize the result to two- or three-dimensional fields. The Fourier power spectrum is given by

$$P(n) = \langle |\delta_n|^2 \rangle, \quad (1)$$

where $\delta_n = (1/L) \int_0^L \delta(x) \exp(-i2\pi nx/L) dx$ and $\langle \dots \rangle$ stands for ensemble average. Similarly, the DWT power spectrum is given by

$$P_j = \langle |\tilde{\epsilon}_{j,l}|^2 \rangle, \quad (2)$$

where $\tilde{\epsilon}_{j,l} = \int_0^L \delta(x) \psi_{j,l}(x) dx$, where $\psi_{j,l}(x)$ is the wavelet function with scale index j and position index l (All the wavelet notations used in this paper are the same as in Fang and

Feng [2000]). For a statistically homogeneous Gaussian field, the right hand side of equation (2) is l -independent.

The Fourier variable δ_n can be expressed by the DWT variable $\tilde{\epsilon}_{j,l}$ as (Fang & Feng 2000)

$$\delta_n = \frac{1}{L} \sum_{j=0}^{\infty} \sum_{l=0}^{2^j-1} \tilde{\epsilon}_{j,l} \hat{\psi}_{j,l}(n) = \sum_{j=0}^{\infty} \sum_{l=0}^{2^j-1} \left(\frac{1}{2^j L} \right)^{1/2} \tilde{\epsilon}_{j,l} e^{-i2\pi n l / 2^j} \hat{\psi}(n/2^j), \quad n \neq 0. \quad (3)$$

where $\hat{\psi}$ is the Fourier transform of the basic wavelet function. Therefore, the Fourier power spectrum is given by

$$P(n) = \frac{1}{L^2} \sum_{j=0}^{+\infty} \sum_{l=0}^{2^j-1} \sum_{j'=0}^{+\infty} \sum_{l'=0}^{2^{j'}-1} \langle \tilde{\epsilon}_{j,l} \tilde{\epsilon}_{j',l'} \rangle \hat{\psi}_{j,l}(n) \hat{\psi}_{j',l'}^\dagger(n) \quad (4)$$

For Gaussian fields, $\langle \tilde{\epsilon}_{j,l} \tilde{\epsilon}_{j',l'} \rangle = P_j \delta_{jj'} \delta_{ll'}$, we have

$$P(n) = \frac{1}{L} \sum_{j=0}^{\infty} P_j \left| \hat{\psi} \left(\frac{n}{2^j} \right) \right|^2. \quad (5)$$

Therefore, the Fourier power spectrum, $P(n)$, and the DWT power spectrum, P_j , are equivalent for Gaussian fields.

Generally, equations (1)–(3) yield

$$P(n) - \frac{1}{L} \sum_{j=0}^{\infty} P_j \left| \hat{\psi} \left(\frac{n}{2^j} \right) \right|^2 = \sum_{j=0}^{+\infty} \sum_{l,l'=0, l \neq l'}^{2^j-1} \langle \tilde{\epsilon}_{j,l} \tilde{\epsilon}_{j,l'} \rangle \hat{\psi}_{j,l}(n) \hat{\psi}_{j,l'}^\dagger(n) + \sum_{j,j'=0, j' \neq j}^{+\infty} \sum_{l=0}^{2^j-1} \sum_{l'=0}^{2^{j'}-1} \langle \tilde{\epsilon}_{j,l} \tilde{\epsilon}_{j',l'} \rangle \hat{\psi}_{j,l}(n) \hat{\psi}_{j',l'}^\dagger(n) \quad (6)$$

The two terms on the right-hand side originate from the non-Gaussianity of the field. That is, the difference between the Fourier and DWT power spectra is a measure of the non-Gaussianity of the field.

2.2. The Fourier and DWT power spectra in the halo model

In the halo model, the developed mass density field $\rho(x)$ is assumed to be a superposition of halos on various scales. It is

$$\rho(x) = \sum_i \rho_i(x - x_i) = \sum_i m_i u(x - x_i, m_i) = \int dx' \sum_i m_i \delta^D(x' - x_i) u(x - x', m_i), \quad (7)$$

where m_i is the mass of halo i , $\delta^D(x)$ is the Dirac delta function, and $u(x - x_i, m_i)$ is the normalized mass density profile of halo i , i.e., $\int dx \rho_i(x - x_i) = \int dx m_i u(x - x_i, m_i) = m_i$. In this case, the DWT variable is

$$\tilde{\epsilon}_{j,l} = (1/\bar{\rho}) \sum_i m_i \int dx u(x - x_i, m_i) \psi_{j,l}(x). \quad (8)$$

The covariance $\langle \tilde{\epsilon}_{j,l} \tilde{\epsilon}_{j,l'} \rangle$ is then given by

$$\langle \tilde{\epsilon}_{j,l} \tilde{\epsilon}_{j,l'} \rangle = \langle \tilde{\epsilon}_{j,l} \tilde{\epsilon}_{j,l'} \rangle^h + \langle \tilde{\epsilon}_{j,l} \tilde{\epsilon}_{j,l'} \rangle^{hh}, \quad (9)$$

where the first and second terms on the right-hand side are usually called one and two halo terms, respectively (Cooray & Sheth 2002). The two-halo term is given by the two-point correlation function of the Gaussian perturbations, and therefore, $\langle \tilde{\epsilon}_{j,l} \tilde{\epsilon}_{j,l'} \rangle^{hh} \simeq 0$, when $l \neq l'$, and the one-halo term, $\langle \tilde{\epsilon}_{j,l} \tilde{\epsilon}_{j,l'} \rangle^h$, is (Feng & Fang 2004)

$$\langle \tilde{\epsilon}_{j,l} \tilde{\epsilon}_{j,l'} \rangle^h = \int dm n(m) \left(\frac{m}{\bar{\rho}} \right)^2 \int dx_1 u(x_1, m) \int dx \int dx' \psi_{j,l}(x) u(x_1 + x - x', m) \psi_{j,l'}(x'), \quad (10)$$

where $n(m)$ is the number density of halos with mass m . Thus, we have

$$\begin{aligned} \langle \tilde{\epsilon}_{j,l} \tilde{\epsilon}_{j,l'} \rangle &= \langle \tilde{\epsilon}_{j,l} \tilde{\epsilon}_{j,l'} \rangle^h \\ &= \frac{1}{2^j} \sum_{n=-\infty}^{\infty} |\hat{\psi}(n/2^j)|^2 \cos[2\pi n(l - l')/2^j] \int dm n(m) \left(\frac{m}{\bar{\rho}} \right)^2 |\hat{u}(n, m)|^2 \end{aligned} \quad (11)$$

where $\hat{u}(n, m) = \int_0^L u(x, m) \exp(-i2\pi nx/L) dx$ is the Fourier transform of the normalized mass profile.

The second term on the right-hand side of equation (6) contains a factor $\hat{\psi}_{j,l}(n) \hat{\psi}_{j,l'}^\dagger(n) \propto \hat{\psi}(n/2^j) \hat{\psi}^\dagger(n/2^{j'}) \simeq 0$, because $n/2^j$ and $n/2^{j'}$ differ by a factor of $2^{|j-j'|}$ if $j \neq j'$, and then, the non-zero ranges of $\hat{\psi}(n/2^j)$ and $\hat{\psi}^\dagger(n/2^{j'})$ do not overlap. Thus, equation (6) yields

$$P(n) - \frac{1}{L} \sum_{j=0}^{\infty} P_j \left| \hat{\psi} \left(\frac{n}{2^j} \right) \right|^2 = L \left(\int dm n(m) \left(\frac{m}{\bar{\rho}} \right)^2 |\hat{u}(n, m)|^2 \right) \sum_{j=0}^{\infty} \left| \hat{\psi} \left(\frac{n}{2^j} \right) \right|^4, \quad (12)$$

where we have used $\sum_{l=0}^{2^j-1} e^{-i2\pi(n-n')l/2^j} = 2^j \delta_{n,n'}$. Equation (12) is the major theoretical result of this paper. Since we know $\sum_{j=0}^{\infty} |\hat{\psi}(n/2^j)|^4$, from the difference between the Fourier and DWT power spectra, one has as a statistical measure

$$U^2(n) = \int dm n(m) \left(\frac{m}{\bar{\rho}} \right)^2 |\hat{u}(n, m)|^2. \quad (13)$$

Since $n(m)$ is the number density of m halos, $U^2(n)$ is an average of the Fourier mode n of mass profile $|\hat{u}(n, m)|^2$ over the ensemble of halos, and the weight of the average is $(m/\bar{\rho})^2$.

2.3. Constraint on halo models with power spectrum

Note that the left hand side of eq.(12) depends only on power spectra of the Fourier modes $P(n)$ and DWT modes P_j , regardless of the definition and selection of particular parameters used in the halo profile and halo mass function. On the other hand, the right hand side of eq.(12) depends on the mass function $n(m)$ and mass profile $\hat{u}(n, m)$ of halos. Therefore, $U^2(n)$ should be invariant with respect to the parameters used for the definition and selection of halos. Thus, $U^2(n)$ provides a general constraint on models of the mass function and mass profile of halos. A reasonable model of the mass function and mass profile of halos must satisfy relation (12). The statistic $U^2(n)$ can be used to compare models with different definitions and selections of halos.

For instance, the universal mass profile of halos generally is assumed to be

$$\rho(r, m) = \frac{\rho_s}{(r/r_s)^\alpha (1 + r/r_s)^\beta}. \quad (14)$$

where the parameters r_s and ρ_s are, respectively, the scale radius and characteristic density of the halo. The index (α, β) is mass independent. It can be $(1, 3)$ of Hernquist (1990), $(1, 2)$ of Navarro et al. (1996), or $(3/2, 3/2)$ of Moore et al. (1999). Obviously, models with different indices (α, β) yield different n -dependences of $\hat{u}(n, m)$. Thus, if one uses the same mass function $n(m)$ for all models (α, β) , $U^2(n)$ will be (α, β) dependent. This is unacceptable. Therefore, in order to match the constraint in eq.(12), for different indices (α, β) , we must use different mass function $n(m)$. In other words, in the halo model, the mass function $n(m)$ of halos actually is halo-shape-parameter dependent. Similarly, the mass function $n(m)$ also depends on the algorithms of halo identification. This point is well-understood in the halo model (Jenkins et al 2001). However, eq.(12) provides an effective tool to test whether the parameters of the halo and halo finder yield a consistent set of halo model ingredients. In other words, the invariance of $U^2(n)$ with respect to the parameters sets a necessary condition of the consistent set of the definition and selection of halo parameters.

3. Samples

To demonstrate the possible application of the statistic $U(n)$, we use the cosmological hydrodynamic simulation samples used in He et al. (2004) and Pando et al. (2004). The samples are produced by the WIGEON (Weno for Intergalactic medium and Galaxy Evolution and formatiON) code, which is a cosmological hydrodynamic/ N -body code based on the Weighted Essentially Non-Oscillatory (WENO) algorithm (Harten et al. 1986; Liu, Osher, & Chan 1994; Jiang & Shu 1996; Shu 1998; Fedkiw, Sapiro & Shu 2003; Shu 2003).

The WENO schemes use the idea of adaptive stencils in the reconstruction procedure based on the local smoothness of the numerical solution to automatically achieve high order accuracy and non-oscillatory properties near discontinuities. Therefore, the WENO algorithm provides a high order precision simulation for fluid with strong shocks.

In a system in which the baryonic gas is gravitationally coupled with dark matter, the temperature of the baryonic gas is generally in the range 10^{4-6} K, and the speed of sound in the baryonic gas is only a few km s^{-1} to a few tens km s^{-1} . On the other hand, the rms bulk velocity of the baryonic gas is on the order of hundreds km s^{-1} (Zhan & Fang 2002). Hence, the Mach number of the gas can be as high as ~ 100 (Ryu et al. 2003). The shocks and discontinuities are extremely strong. The WENO code for cosmology has passed necessary tests including the Sedov blast wave and the formation of the Zeldovich pancake (Feng, Shu, & Zhang 2004). It has been successfully used to produce the QSO Ly α transmitted flux (Feng, Pando, & Fang 2003). The statistical features of these samples are in good agreement with observed features not only on second order measures, like the power spectrum, but also up to orders as high as eighth for the non-Gaussian behavior (Pando, Feng, & Fang 2002). Hence we believe that the WENO samples would be suitable to study the non-Gaussian feature of the mass field with the statistic $U(n)$.

The simulations were performed in a periodic, cubic box of size $25 h^{-1}\text{Mpc}$ with a 192^3 grid and an equal number of dark matter particles. The simulations start at a redshift $z = 49$. The linear power spectrum is taken from the fitting formulae presented by Eisenstein & Hu (1998). The baryon fraction $f_c = \bar{\rho}_b/\bar{\rho}_{dm} = \Omega_b/\Omega_{dm}$ is fixed using the constraint from primordial nucleosynthesis as $\Omega_b = 0.0125h^{-2}$ (Walker et al. 1991). A uniform UV-background of ionizing photons is assumed to have a power-law spectrum of the form $J(\nu) = J_{21} \times 10^{-21} (\nu/\nu_{HI})^{-\alpha} \text{erg s}^{-1} \text{cm}^{-2} \text{sr}^{-1} \text{Hz}^{-1}$, where the photoionizing flux is normalized by the parameter J_{21} at the Lyman limit frequency ν_{HI} and is suddenly switched on at $z > 10$ to heat the gas and reionize the universe. The atomic processes, including ionization, radiative cooling and heating, are modeled in the same way as in Cen (1992) in a plasma of hydrogen and helium of primordial composition ($X = 0.76$, $Y = 0.24$). The processes such as star formation, and feedback due to SN and AGN activities have not yet been taken into account.

For statistical studies, we randomly sampled 500 one-dimensional fields from the simulation results at redshift $z = 0$. Each one-dimensional sample, of size $L=25 h^{-1}\text{Mpc}$, contains 192 data points, every one of which contains mass densities of dark matter and baryonic gas.

4. Applications

4.1. The discrepancy of baryonic gas from the dark matter

It has been well known that in the nonlinear regime the clustering of baryonic gas will decouple from the underlying dark matter (e.g., He et al. 2005; Kim et al 2005). For instance, Figure 1 plots two-dimensional contours of the baryonic gas and dark matter densities. One can see a halo of the scale $\sim 5 h^{-1}$ Mpc at the lower part of the plots. The size of the $\rho_b/\bar{\rho}_b > 1$ region is obviously larger than the dark matter counterpart at $\rho/\bar{\rho} > 1$. It means that much baryonic gas remains outside the halo. This is a discrepancy of baryonic gas from the dark matter. Although the discrepancy can be directly seen by eye, a quantified measure is still necessary. The discrepancy is significant in massive halos. One can have a quantified measure of the discrepancy of the massive halos. However, a measure of the discrepancy over the whole field is also necessary. The latter can be done with the statistic in eq.(12).

Similar to eq.(7), the mass field of baryonic gas in the halo model can be written as

$$\begin{aligned}\rho_b(x) &= \sum_i \rho_{i,b}(x - x_i) = \sum_i m_i f(m_i) u^b(x - x_i, m_i) \\ &= \int dx' \sum_i m_i f(m_i) \delta^D(x' - x_i) u_b(x - x', m_i),\end{aligned}\tag{15}$$

where $\rho_{i,b}(x - x_i)$ is the mass profile of baryonic gas in the halo i , $u_b(x - x_i, m_i)$ is the normalized baryon mass profile of the halo with dark matter mass m_i , i.e. $\int dx u_b(x - x_i, m_i) = 1$, and $f(m_i) = m_b/m_i$ is the baryon fraction of the halo with mass m_i . Thus, with a similar procedure as in §2, we can show that the difference between the Fourier and DWT power spectra of the mass field in eq.(15) gives a measurement of baryonic gas in halos as

$$\begin{aligned}U_b^2(n) &= \int dm n(m) \left(\frac{m_b}{\rho_b}\right)^2 |\hat{u}_b(n, m)|^2 \\ &\quad \int dm n(m) \left(\frac{m}{\rho}\right)^2 \left(\frac{f(m)}{f_c}\right)^2 |\hat{u}_b(n, m)|^2,\end{aligned}\tag{16}$$

where $\hat{u}_b(n, m)$ is the Fourier transform of $u_b(x)$, and $f_c = \Omega_b/\Omega_{dm}$.

If the distribution of baryonic gas is given by a similarity mapping of dark matter (e.g., Kaiser 1986), i.e. $\rho_b(x) = f_c \rho(x)$, we will have $U^2(n) = U_b^2(n)$. Thus, any difference between $U^2(n)$ and $U_b^2(n)$ will indicate the violation of the similarity mapping between baryon gas and dark matter. The difference may originate from the two factors: (1) the normalized mass profiles $u_b(x)$ are different from those of the dark matter $u(x)$, and (2) the baryon fraction $f(m)$ is not always equal to the cosmic value f_c , but is m -dependent.

For the hydrodynamic simulation samples of §3, the results of $U_b(n)$ and $U(n)$ are shown in Figure 2. The error bars in Figure 2 indicate the 68% confidence level estimated by the bootstrap method. Figure 2 shows that $U_b(n)$ is always lower than $U(n)$ in the range $n \geq 2$. For each data point at n , the mean values of $U_b(n)$ and $U(n)$ are also derived by bootstrap re-sampling from the 500 samples. Thus, we can do a t -test at every n to assess the significance of the deviation of $U(n)$ from $U_b(n)$. We find that the significance of $U_b(n)$ to be different from $U(n)$ is greater than 99% with a t -test for every n in the range 5 to 15. The result $U_b(n) < U(n)$ means that the mean baryon fraction on scale L/n should be lower than f_c . Therefore, from Figure 2 one can conclude that the baryon fraction within a few Mpc surrounding a halo is less than f_c . Thus, more baryonic matter remains outside the collapsed objects. This point can be seen clearly from the right panel of Figure 3, which shows that f/f_c is lower than 1 at the central part of this halo, while the contours of $f/f_c > 1$ are outside the central part. Observations also showed that the baryon fraction in galaxy clusters seems to be lower than the result of primordial nucleosynthesis (Ettori et al. 2004).

As mentioned above, the statistic $U-U_b$ gives a quantitative measurement of this feature with the entire mass field, not from individual halos. Moreover, if the relation between profiles of baryonic gas $\rho_b(x)$ and dark matter $\rho(x)$ can be described by a nonlocal bias model, i.e. $\rho_b(x) = \int b(x-x')\rho(x')dx$, where $b(x-x')$ is the bias function, we have $U_b(n) = b(n)U(n)$. Therefore the statistic $U-U_b$ can be used to detect the biased distribution of baryonic gas, and the ensemble averaged nonlocal bias function in Fourier space.

4.2. Reconstruction of mass density profiles

We now consider the problem of recovering the mass profile. Since $U(n)$ is weight-averaged, from $U(n)$ we cannot get $\hat{u}(n, m)$ for each given mass. However, the weight factor is $n(m)m^3 d \ln m \propto [m/m_{col}(z)]^{3-\mu} \exp[-m/m_{col}(z)] d \ln m$, and $3 - \mu > 1$. The maximum of the weight is at $\simeq m_{col}(z)$. Hence, $U(n)$ is approximately equal to $|\hat{u}(n, m)|$, where the logarithm mass $\ln m$ is within the range $\ln m_{col} \pm \Delta \ln m$, and $\Delta \ln m \simeq 1$.

We can reconstruct the mass density profile $u(x)$ by a Fourier transform as

$$u(x) \propto U(x) = \frac{2}{L} \sum_{n=1}^N U(n) \cos(2\pi nx/L). \quad (17)$$

In eq. (17) N is dependent on the sample resolution. Since $u(x) = 0$ at large x , and therefore, $U(n=0) = 0$. Using the $U(n)$ of dark matter shown in Figure 2, we have $U(x)$ given in Figure 4. The error bar is also estimated by the bootstrap method. First, we see that in Figure 4, there is a region with non-physical density $U(x) < 0$. This is because of the absence

of the power on scales that are comparable to or larger than the size of the simulation box. Second, we do not have the information of the mass profile on scales less than $0.2 h^{-1}$ Mpc, which is limited by the resolution of the sample. Nevertheless, Figure 4 already shows some interesting properties, which are different from those of the mass density profile given by an average of individual halos.

First, we fit $U(x)$ by the mass profile of Eq.(14). For $(\alpha, \beta) = (1, 2)$ and $(1, 3)$, the corresponding one-dimensional profile is then

$$u(x) \propto \frac{1}{(1 + |x/r_s|)^{\beta-\alpha}}. \quad (18)$$

The fitting results are shown in Figure 4. The values of scale radii r_s are, obviously, in the sense of a statistical average over the field. It should be pointed out that the fitting done in Figure 4 is to cover a range as large as $6 h^{-1}$ Mpc. This is because the $U(x)$ provides a measurement of the entire mass field. The fitting profile is also an ensemble averaged measurement of the entire mass field.

Figure 4 shows that the fitting curves for $(\alpha, \beta) = (1, 2)$ and $(1, 3)$ are about the same. That is, both fitting curves have about the same goodness-of-fit. However, the parameters of r_s for $(\alpha, \beta) = (1, 2)$ and $(1, 3)$ are very different. The former is $0.2 h^{-1}$ Mpc, while the latter is $0.7 h^{-1}$ Mpc. For the model $(\alpha, \beta) = (1, 2)$, the scale radii of halo with mass $m_{col} \simeq 10^{13} M_{\odot}$, is found to be $r_s \simeq 0.06 h^{-1}$ Mpc (Bullock et al. 2001). It is much smaller than $0.2 h^{-1}$ Mpc. This is probably because that the number $0.2 h^{-1}$ Mpc is close to the sample resolution. We may miss some halos with small r_s . However, there is also a physical reason leading to $r_s > 0.06 h^{-1}$ Mpc. The profile of halos is found to be sensitive to the dynamical status (Jing 2000). With an unbiased selection of all massive halos from N -body simulations, it has found that, for the LCDM model, there are only about 44% of the halos than can be fitted by the profile (14) of $(\alpha, \beta) = (1, 2)$ with a fitting residual $dvi_{max} < 0.15$. These halos are well virialized. About 40% of halos have $0.15 < dvi_{max} < 0.30$, and 16% have $dvi_{max} > 0.30$. The latter has obvious sub-structures. The parameter r_s increases with dvi_{max} . The value of r_s of $dvi_{max} > 0.3$ halos are larger than those of $dvi_{max} < 0.15$ halos by a factor of about 2. Therefore, in the case of $(\alpha, \beta) = (1, 2)$, the parameter of mass profile given by the $U(n)$ recovery is basically reasonable. It is an ensemble averaged parameter over virialized as well as sub-structured halos.

On the other hand, for the case of $(\alpha, \beta) = (1, 3)$, $r_s = 0.7 h^{-1}$ Mpc is too large. This is probably because that the measure $U(n)$ is over the whole mass field, and therefore, it is more sensitive to the tail of the profile eq.(18). The tail of the $(\alpha, \beta) = (1, 3)$ profile, $1/r^4$ (or in one dimension $1/x^2$) is more steep than that of $(\alpha, \beta) = (1, 2)$, $1/r^3$ (or in one-dimension $1/x$). Thus, the fitting by $(\alpha, \beta) = (1, 3)$ yields a large value of r_s . Therefore,

the $U(n)$ recovery of the mass profile indicates that the profiles $(\alpha, \beta) = (1, 3)$ may not be representative of LCDM halos.

5. Discussions and conclusions

In the Fourier representation, the essential difference between the Gaussian field and the halo-filled field is in the distribution of phases in Fourier modes. As coherent structures, the phases of the density perturbations of halos are highly correlated, while the phases of the Gaussian field are random, or uncorrelated. On the other hand, the covariance of the Fourier modes is not sensitive to the phases of perturbations, while the DWT covariance contains information about both scale and position, which is phase-sensitive. Therefore, even with second-order statistics of Fourier and DWT modes (in the current case, it is the difference between their power spectra), one can effectively draw information about halos.

We show that, in the halo model of large-scale structure formation, the difference between the Fourier and the DWT power spectra provides a statistical measurement of the halos. This method has all the advantages of power spectrum statistics, since it directly reflects the physical scales of the clustering processes that affect structure formation. Mathematically, the positive definiteness of the power spectrum is useful for constraining the parameter space. Moreover, it would also be easy to estimate the effect of redshift distortion. For instance, the linear redshift distortions of the Fourier and the DWT power spectra are the same (Yang et al. 2001; Zhan & Fang 2003). Therefore, the Fourier - DWT power spectrum difference is free from linear redshift distortions. In the halo model, non-linear redshift distortions come from halos. Thus, the Fourier - DWT power spectrum difference depends only on the redshift distortions given by halos. This would be useful for studying the velocity profile of halos.

This statistic is invariant with respect to various models with reasonably defined and selected parameters of the halo models. Therefore, it is a constraint for a consistent set of halo model ingredients. This feature is useful for extracting information of halos, containing both virialized halos and halos with significant sub-structures. This cannot be done with the identification of halos. This statistic measurement is on the whole map of various structures, such as galaxies, quasars, Ly-alpha absorption transmission, etc., and therefore, it would be easy to handle various selections.

With the measurement of $U(n)$, we may investigate the bias of baryonic gas with respect to dark matter. In particular, the two types of the bias, (1) $u_b(x) \neq u(x)$, and (2) $f_c(m) \neq f_c$ would be distinguishable with $U(n)$. This method can also be used to detect the difference

of spatial distributions of different objects of the universe.

In this paper, we only considered one-dimensional problems. In the three-dimensional case, the DWT power spectrum contains both diagonal and non-diagonal modes. It has been shown that the power spectra of the diagonal and non-diagonal modes are effective in detecting different clustering feature (Yang et al 2001). Therefore, the difference between three-dimensional Fourier and DWT power spectra would provide more constraints and information on halo models of the cosmic mass field in the nonlinear regime.

We thank the anonymous referee for a stimulating report. P.H. is supported by a Fellowship of the World Laboratory. L.L.F. acknowledges support from the National Science Foundation of China (NSFC) and the National Key Basic Research Science Foundation. This work is partially supported by the National Natural Science Foundation of China (10025313) and the National Key Basic Research Science Foundation of China (NKBRSF G19990752).

REFERENCES

- Bullock, J.S., Kolatt, T. S., Sigad, Y., Somerville, R.S., Kravtsov, A.V., Klypin, A.A., Primack, J.R., & Dekel, A. 2001, MNRAS, 321, 559
- Cen, R. 1992, ApJS, 78, 341
- Cooray, A., & Sheth, R. 2002, Physics Reports, 372, 1
- Eisenstein, D. & Hu, W., 1998, ApJ, 496, 605
- Ettori, S., Borgani, S., Moscardini, L., Murante, G., Tozzi, P., Diaferio, A., Dolag, K., Springel, V., Tormen, G., & Tornatore, L. 2004, MNRAS, 354, 111
- Fang, L.Z., & Feng, L.L. 2000, ApJ, 539, 5
- Fedkiw, R.P., Sapiro, G., & Shu, C.W. 2003, J. Comput. Phys., 185, 309
- Feng, L.L., Pando, J., & Fang, L.Z. 2003, ApJ, 587, 487
- Feng, L.L., & Fang, L.Z. 2004, ApJ, 601, 54
- Feng, L.L., Shu, C.W., & Zhang, M.P. 2004, ApJ, 612, 1
- Harten, A., Osher, S., Engquist, B., & Chakravarthy, S. 1986, Applied Numerical Mathematics, 2, 347
- He, P., Feng, L.L., & Fang, L.Z. 2004, ApJ, 612, 14
- He, P., Feng, L.L., & Fang, L.Z. 2005, ApJ, 623, 601

- Hernquist, L. 1990, ApJ, 356, 359
- Jenkins, A., Frenk, C.S., White, S., Colberg, J.M., Cole, S. Evard, A., Couchman, H.M., & Yoshida, N. 2001, MNRAS, 321, 372
- Jiang, G., & Shu, C.W. 1996, J. Comput. Phys., 126, 202
- Jing, Y.P. 2000, ApJ, 535, 30
- Kaiser, N. 1986, MNRAS, 222, 323
- Kim, B, He, P., Pando, J., Feng, L.L & Fang, L.Z. ApJ, in press, astro-ph/0502175
- Liu, X.-D, Osher, S. & Chan, T. 1994, J. Comput. Phys., 115, 200
- Moore et al. 1999, MNRAS, 310, 1147
- Navarro, J., Frenk, C., & White, S. 1996, ApJ, 462, 563
- Neyman, J., & Scott, E.L. 1952, ApJ, 116, 144
- Pando, J., Feng, L.L., & Fang, L.Z. 2004, ApJS, 154, 475
- Peebles, P.J.E. 1980, The Large-Scale Structure of the Universe. Princeton Univ. Press, Princeton
- Ryu, D., Kang, H., Hallman, E., & Jones, T.W. 2003, ApJ, 593, 599
- Scherrer, R.J., & Bertschinger, E. 1991, ApJ, 381, 349
- Shu, C.W. 1998, in Advanced Numerical Approximation of Nonlinear Hyperbolic Equations, Ed. A. Quarteroni, Lecture Notes in Mathematics, (Springer), 1697, 325
- Shu, C.W. 2003, Int. J. Comput. Fluid Dyn., 17, 107
- Walker, T.P., Steigman, G., Kang, H.S., Schramm, D.M., & Olive K.A. 1991, ApJ, 376, 51
- Wang, Y., Yang, X.H., Mo, H.J., van den Bosch, F.C., & Chu, Y.Q. 2004, MNRAS, 353, 287
- Yang, X.H., Feng, L.L., Chu, Y.Q., & Fang, L.Z. 2001, ApJ, 553, 1
- Zhan, H., & Fang, L.Z. 2002, ApJ, 566, 9
- Zhan, H., & Fang, L.Z. 2003, ApJ, 585, 12

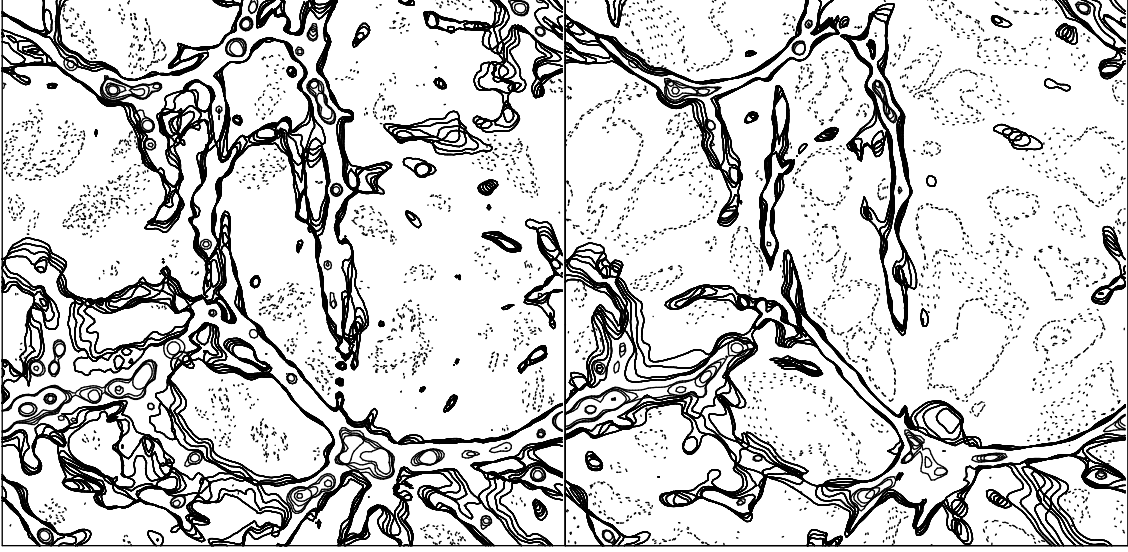


Fig. 1.— Baryonic gas (left) and dark matter (right) density contour plots for a slice of $0.26 \, h^{-1} \, \text{Mpc}$ thickness at $z = 0$. The solid contours represent overdense regions with $\rho/\bar{\rho} > 1$. The dotted lines represent underdense regions with $\rho/\bar{\rho} < 1$.

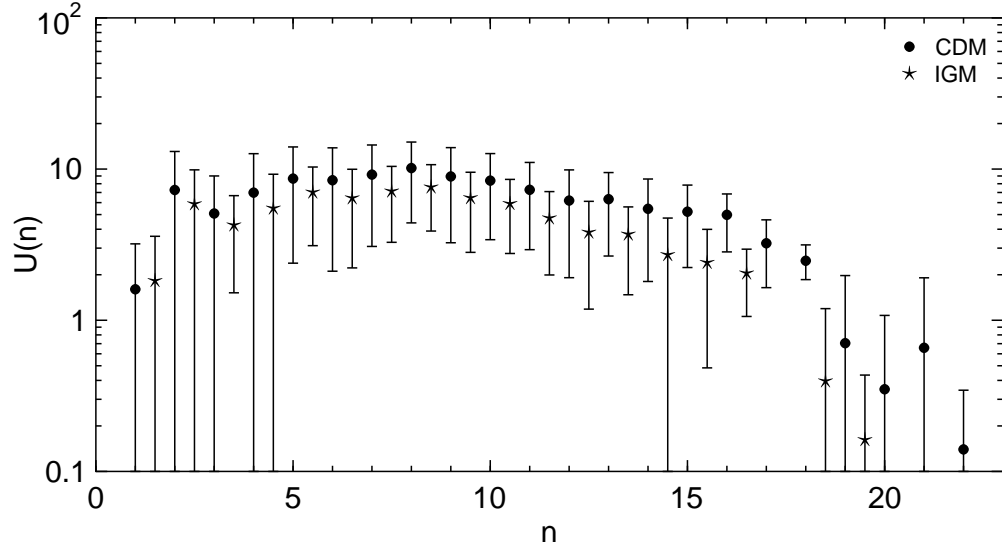


Fig. 2.— The statistical measurements $U(n)$ (filled circle) and $U_b(n)$ (star) versus n . For clarity, $U_b(n)$ is right-shifted for half unit. The error bars are estimated by the bootstrap method

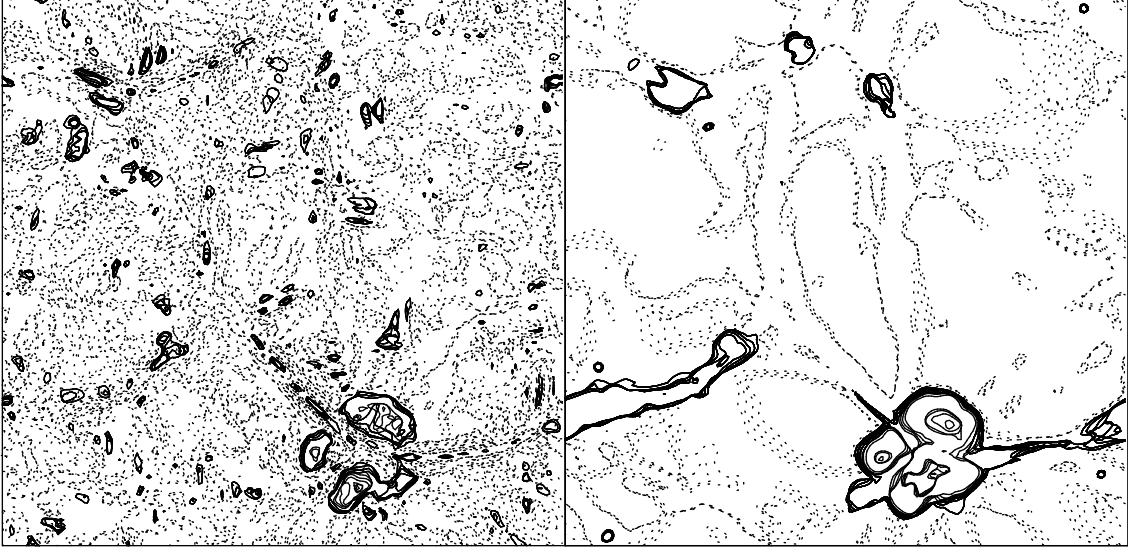


Fig. 3.— Temperature (left) and baryon-to-dark matter ratio (right) contour plots for a slice of $0.26 \, h^{-1} \, \text{Mpc}$ thickness at $z = 0$. The solid contours represent, respectively, regions with $T > 10^5 \, \text{K}$ (left) and $\rho_b/\rho > f_c$ (right). The dotted lines represent $T < 10^5 \, \text{K}$ (left) and $\rho_b/\rho < f_c$ (right).

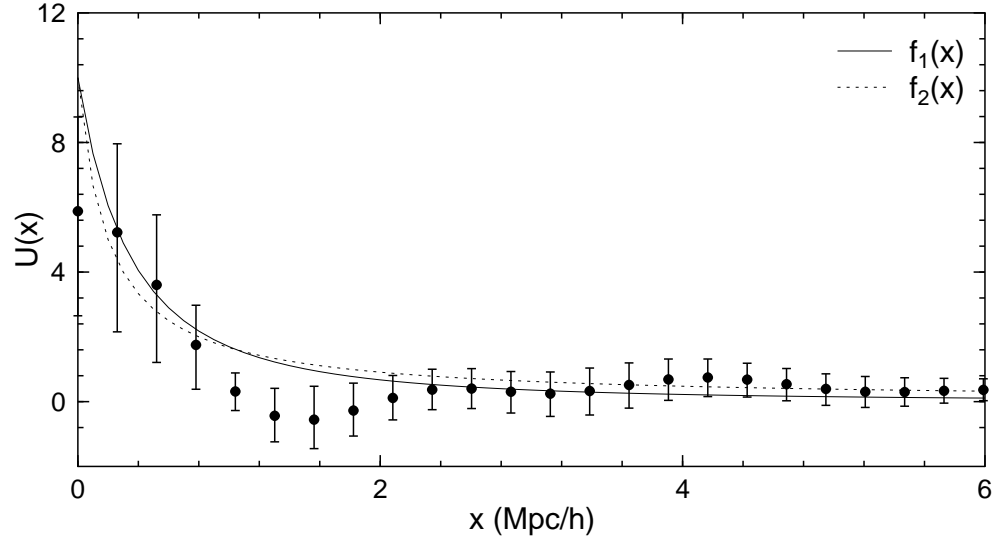


Fig. 4.— Mass density profile $U(x)$ in physical space. The fitting curves are given by equation (17) with $(\alpha, \beta) = (1, 3)$ (solid line) and $(1, 2)$ (dashed line).